

FoV and Efficiency Optimization for Resonant Beam SLIPT with Telescope Integration

Shun Han, Mingliang Xiong, Mengyuan Xu, Zeqian Guo, Wen Fang, and Qingwen Liu, *Senior Member, IEEE*

Abstract—Meeting the large bandwidth demands of wireless communication for mobile Internet of Things (IoT) devices while enhancing their endurance is a significant challenge. Simultaneous lightwave information and power transfer (SLIPT) technology offers the potential to realize wireless charging and signal transfer, making it suitable for supporting autonomous vehicles and drones. The resonant beam system (RBS) leverages the self-aligning property of a spatially distributed laser resonator (SSLR), allowing energy transmission from the transmitter to the receiver without mechanical alignment. However, the existing resonant beam SLIPT system exhibits a limited field of view (FoV) and transmission efficiency, facing challenges in practical applications. In this paper, we propose a resonant beam SLIPT system enhanced by incorporating an internal telescope and optimizing the communication, energy transfer, and FoV performance by solving the Pareto front set of the system’s achievable performance region. The results indicate that the optimized FoV is increased by 17%, reaching $\pm 26.8^\circ$, while its average end-to-end efficiency is improved by 145%, achieving 5.4%.

Index Terms—Simultaneous lightwave information and power transfer, FoV, resonant beam, retro-reflector, spatially distributed laser resonator.

I. INTRODUCTION

Simultaneous lightwave information and power transfer (SLIPT) have attracted wide attention in extending the battery lifetime and providing wireless communication connection of energy-constrained terminal equipment (e.g., smartphones, electric vehicles, robots, drones, etc) [1–3]. Additionally, it is regarded as a candidate solution for facilitating the transition to the 6G era and advancing sustainable Internet of Things (IoT) technologies [4]. SLIPT utilizes light-emitting diodes (LEDs) or lasers to enable wireless connection with mobile devices, offering the benefits of a broader communication bandwidth while providing a continuous power supply to these devices.

Integrating energy harvesting modules into the optical wireless communication (OWC) systems enables the implementation of SLIPT technology. The most promising OWC technologies include visible light communication (VLC), light fidelity (LiFi), optical camera communication (OCC), free-space optics (FSO), and resonant beam systems (RBS) [5–

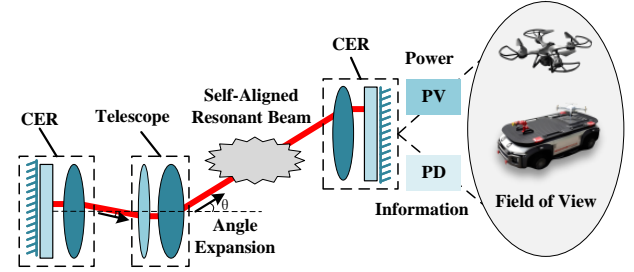


Fig. 1. The example of application scenario for resonant beam SLIPT system.

9]. Among these, VLC and LiFi technologies utilize divergent light sources, such as LEDs and LDs, to provide communication rates of up to 100 Gbps to the receiver and indoor illumination [10]. Combined with energy harvesting technology, these systems can charge receiving devices [11, 12]. However, their energy transmission efficiency is constrained by the receiver size and beam energy density, typically reaching only milliwatt level [13, 14]. OCC technology offers compatibility with AR and VR platforms, enabling offline video, audio, and text sharing between users [15]. However, it has limited communication rates and faces difficulties in energy harvesting [16]. FSO technology uses collimated lasers as the transmission carrier and can achieve high-speed wireless communication and high-power energy transfer [17]. Nevertheless, it requires acquisition, tracking, and pointing (ATP) mechanisms to compensate for alignment errors, making it economically inefficient for the IoT system [18].

Although SLIPT technologies hold significant potential, they face two major challenges: transmitting high power within eye-safe standards and achieving adequate reception despite limited receiver size [19, 20]. The resonant beam system (RBS), as a promising 6G technology, utilizes frequency-doubled technology to separate the communication beam and power transmission beam, thereby avoiding echo interference and enabling both high-speed communication and high-power energy transfer [21–24]. As shown in Fig. 1, RBS can transmit energy and information to devices within the field of view (FoV) coverage area. Compared to other OWC systems, the RBS system benefits from its SSLR design, which provides mobile self-alignment features and inherent human safety [25–27]. RBS protection light design can also enhance the system’s safety, allowing for higher power energy transmission within human safety standards. However, several issues still constrain the development of RBS systems. Firstly, the system’s FoV is limited. The FoV determines the range within which the

S. Han, M. Liu, M. Xu, Z. Guo, and Q. Liu are with the College of Electronic and Information Engineering, Tongji University, Shanghai 201804, China (e-mail: hanshun@tongji.edu.cn, xumy@tongji.edu.cn, guozeqian@tongji.edu.cn and qliu@tongji.edu.cn).

M. Xiong is with Hangzhou Institute of Extremely-Weak Magnetic Field Major National Science and Technology Infrastructure, Hangzhou 310052, China (email:xiongml@foxmail.com).

W. Fang is with the School of Electronic Information and Electrical Engineering, Shanghai Jiao Tong University, Shanghai 200240, China (e-mail: wendyfang@sjtu.edu.cn).

system's receiver can move. Some studies have redesigned the RBS system's transceiver structure, achieving an FoV of ± 5 degrees, yet this remains significantly smaller compared to VLC and LiFi technologies [24]. Secondly, the end-to-end transmission efficiency of RBS requires improvement. In [28], the adoption of aspheric lenses to correct the spherical aberration increased the laser efficiency to 36%, but at the cost of reducing the system's FoV [29]. In [30], an optimized asymmetric cavity design was proposed to enhance the RBS system's end-to-end efficiency effectively. However, this optimization method did not account for the impact on the FoV.

This paper proposes a resonant beam SLIPT system incorporating a telescope within the cavity. This integration allows for adjusting the FoV and transmission efficiency of the resonant beam SLIPT system. We also design a novel resonant beam SLIPT system. By optimizing the placement of the modulator and gain medium, we achieve a more rational design of the resonant cavity. Furthermore, We optimize the resonant beam SLIPT system with an internal telescope by refining the structural parameters of the SSLR. This optimization yields the Pareto frontier of the system's achievable performance range, enhancing the FoV and the average optical transmission efficiency compared to the system before optimization. The contributions of our work are as follows:

- 1) We design a novel SSLR structure by introducing an internal telescope, separating the modulator and gain medium in the RB-SLIPT system. This design can adjust the transmission efficiency and FoV of the system and simplify the overall system architecture.
- 2) We formulate and solve the optimization of the dedicated system to maximize the powering and FoV performance while ensuring stable communication. The results show that the optimized system achieves a maximum FoV of $\pm 26.8^\circ$ with an average end-to-end transmission efficiency of 5.4%.

The remainder of this paper is organized as follows. Section II introduces an RB-SLIPT system with an internal telescope structure. We analyze the system's energy transmission power and communication rate when the receiver is in motion. In Section III, we propose an optimization method based on the RB-SLIPT system and solve for the Pareto frontier of the system's achievable performance region. Section IV analyzes the optimized system's performance enhancements and the trade-off between power transfer and communication. Finally, we conclude in Section V.

II. SYSTEM MODEL

A. RB-SLIPT Structure

The resonant beam communication scheme using frequency-doubled beams for simultaneous energy and data transmission was first proposed in [31]. By employing frequency separation to distinguish between the power transfer and communication beams, the impact of echo interference on communication can be effectively eliminated [32]. In this paper, we optimize the resonant beam SLIPT system design by incorporating a telescope at the transmitter based on the design of the frequency-doubled RBS communication system.

As shown in Fig. 2(b), the telescope is an optical module consisting of two lenses. The incident angle θ_2 of the beam entering from the side with the shorter focal length lens will always be greater than the exit angle θ_1 of the beam leaving from the other side of the telescope, and the relationship always satisfies

$$\left| \frac{\theta_1}{\theta_2} \right| = \left| \frac{f_4}{f_3} \right|, \quad (1)$$

where f_3 and f_4 are the focal lengths of the lenses L3 and L4 in the telescope. Moreover, when the telescope is placed in an appropriate position within the SSLR, the resonant beam will always pass through two points in the telescope: the anterior focal point of the front lens, denoted as point a , and the posterior focal point of the rear lens, denoted as point b . We refer to these points as the pupil, through which the resonant beam consistently passes. Since we introduced a telescope into the SSLR, an additional pupil appeared in the system, which can be used to place optical devices. Therefore, we separate the modulator and the gain medium to build a more straightforward resonant beam SLIPT system, as shown in Fig. 2. Inside the SSLR are three different wavelengths of light beams: the resonant beam for energy transmission, the frequency-doubled beam for communication, and the pump beam. When the pump light illuminates the gain medium, the resonant beam is generated through the stimulated emission process in the SSLR. The resonant beam oscillates back and forth in the SSLR until the mode stabilizes. The stable resonant beam is then emitted through the output mirror M2, passes through the dichroic mirror M3, and is converted into electrical energy by a photovoltaic (PV) cell. The frequency-doubled beam is generated when the resonant beam passes through a second harmonic generation (SHG) crystal. The frequency-doubled beam is modulated using an electro-optic modulator (EOM) and subsequently reflected by mirror M3 into a photodetector (PD), converted into electric signals.

B. System stability analysis

The resonant beam SLIPT system operates only within the stable range of the SSLR. Therefore, it is essential to determine the stable range to ensure the designed system parameters are both rational and practical. The transmitter of the SSLR consists of a telecentric cat's eye and a telescope. Through ABCD matrix analysis, the ray transfer matrix of the telecentric CER can be obtained as

$$\mathbf{M}_{\text{CER}} = \begin{bmatrix} 1 & 0 \\ -\frac{1}{f_{\text{R}}} & 1 \end{bmatrix} \begin{bmatrix} -1 & 0 \\ 0 & -1 \end{bmatrix}, \quad (2)$$

where

$$f_{\text{R}} = \frac{f^2}{2(l-f)}, \quad (3)$$

f is the lens's focal length in the telecentric CER, and l is the interval between the mirror and the lens in the telecentric CER. Since an additional telescope is included at the transmitter of

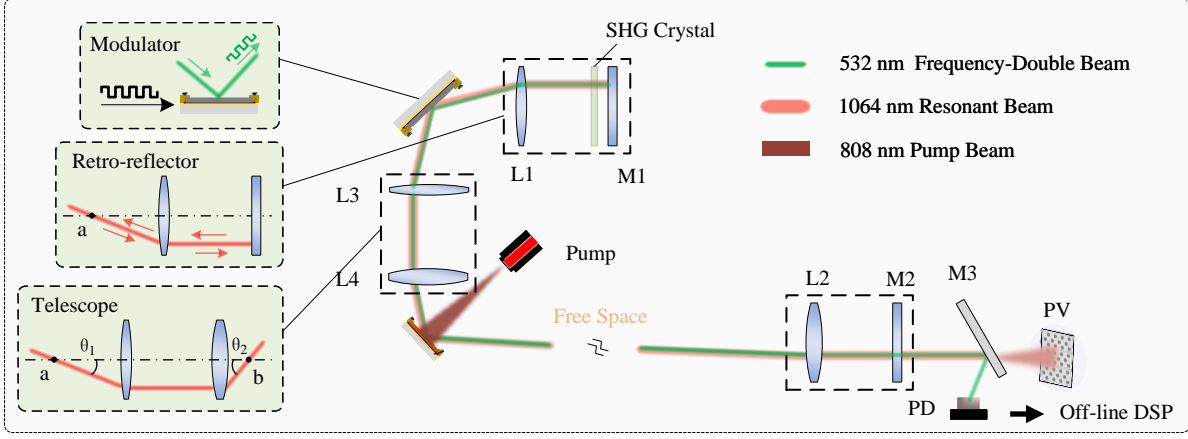


Fig. 2. schematic diagram of resonant beam SLIPT system design with an internal telescope. (PD: photodiode; PV: photovoltaic)

the system, the ray transfer matrix of the system's transmitter can be expressed as

$$\mathbf{M}_{\text{tx}} = \mathbf{M}_{\text{tele}}^T \mathbf{M}_{\text{CER}} \mathbf{M}_{\text{tele}} = \begin{bmatrix} 1 & 0 \\ -\frac{f_3^2}{f_{R1}f_4} & 1 \end{bmatrix} \begin{bmatrix} -1 & 0 \\ 0 & -1 \end{bmatrix}, \quad (4)$$

$$\mathbf{M}_{\text{tele}} = \begin{bmatrix} 1 & f_3 \\ 0 & 1 \end{bmatrix} \begin{bmatrix} 1 & 0 \\ -\frac{1}{f_3} & 1 \end{bmatrix} \begin{bmatrix} 1 & f_3 + f_4 \\ 0 & 1 \end{bmatrix}, \quad (5)$$

$$\mathbf{M}_{\text{tele}}^T = \begin{bmatrix} 1 & f_4 \\ 0 & 1 \end{bmatrix} \begin{bmatrix} 1 & 0 \\ -\frac{1}{f_4} & 1 \end{bmatrix} \begin{bmatrix} 1 & f_3 + f_4 \\ 0 & 1 \end{bmatrix}, \quad (6)$$

To ensure that the FoV of the CER and the telescope at the transmitter of the system match, it is necessary to satisfy $f_1 = f_3$. Furthermore, if we let $\Delta_1 = l_1 - f_1$, $\Delta_2 = l_2 - f_2$, and $M_t = f_3/f_4$, the ray transfer matrices of the transmitter \mathbf{M}_{tx} and the receiver \mathbf{M}_{rx} can be expressed as

$$\mathbf{M}_{\text{tx}} = \begin{bmatrix} 1 & 0 \\ -1/\frac{f_3^2}{2\Delta_1 M_t^2} & 1 \end{bmatrix} \begin{bmatrix} -1 & 0 \\ 0 & -1 \end{bmatrix}, \quad (7)$$

$$\mathbf{M}_{\text{rx}} = \begin{bmatrix} 1 & 0 \\ -1/\frac{f_2^2}{2\Delta_2} & 1 \end{bmatrix} \begin{bmatrix} -1 & 0 \\ 0 & -1 \end{bmatrix}. \quad (8)$$

According to Equation (2), it can be found that the transmitter can be equivalently regarded as a telecentric CER with an effective focal length $f_{R1} = \frac{f_1^2}{2\Delta_1 M_t}$ and the receiver is a telecentric CER with an effective focal length $f_{R2} = \frac{f_2^2}{2\Delta_2}$. Therefore, the entire system can be considered as an SSLR composed of two asymmetric telecentric CERs. Using the effective focal lengths f_{R1} and f_{R2} , the single-pass transmission

matrix of the SSLR can be further simplified from Equation (8) from [33] as

$$\mathbf{M}_s = \begin{bmatrix} -\frac{\Delta_2}{f_2} & f_2 \\ -\frac{1}{f_2} & 0 \end{bmatrix} \begin{bmatrix} 1 & d \\ 0 & 1 \end{bmatrix} \begin{bmatrix} 0 & -f_4 \\ \frac{1}{f_4} & \frac{\Delta_1}{f_4} \end{bmatrix}, \quad (9)$$

$$= \begin{bmatrix} \frac{\Delta_2(2f_{R2}-d)}{f_4 f_2} & \frac{\Delta_1 \Delta_2}{f_4 f_2} (2f_{R2}-d) + \frac{\Delta_2 f_1}{f_2} \\ -\frac{d}{f_4 f_2} & \frac{\Delta_1(2f_{R1}-d)}{f_4 f_2} \end{bmatrix},$$

while

$$\begin{cases} g_1^* = \frac{\Delta_2(2f_{R2}-d)}{f_4 f_2} \\ g_2^* = \frac{\Delta_1(2f_{R1}-d)}{f_4 f_2} \end{cases}. \quad (10)$$

Based on the single-pass transmission matrix \mathbf{M}_s , the stability conditions of the RBS can be obtained by solving the resonant cavity stability condition $0 < g_1^* g_2^* < 1$ [34].

C. Resonant beam radius calculation

The beam radius is an important parameter of the resonant beam, which determines the diffraction loss of the resonant beam passing through each optical module in the cavity, as well as the pumping efficiency of the pump light. The radius of curvature of the equi-phase plane and the beam radius of the resonant beam at any position in the separated resonant cavity can be expressed by introducing the q-parameter of the Gaussian beam [35]

$$\frac{1}{q(z)} = \frac{1}{R(z)} - \frac{i\lambda}{\pi\omega_{00}^2(z)}, \quad (11)$$

where λ is the wavelength of the resonant beam, $R(z)$ and $\omega_{00}(z)$ are the radius of curvature of the equi-phase plane and beam radius of the resonant beam at the propagation distance z , respectively. When $z = 0$, we can obtain the q-parameter of the resonant beam at mirror M1 $q(0)$. Since mirror M1 is a plane mirror and the radius of curvature of the intra-cavity resonant beam at the mirror is always equal to the mirror's radius of curvature, we can obtain $\frac{1}{R(0)} = 0$. Thus the q-parameter of the resonant beam at M1 $q(0)$ is given by

$$q(0) = \frac{i\pi\omega_{00}^2(0)}{\lambda}, \quad (12)$$

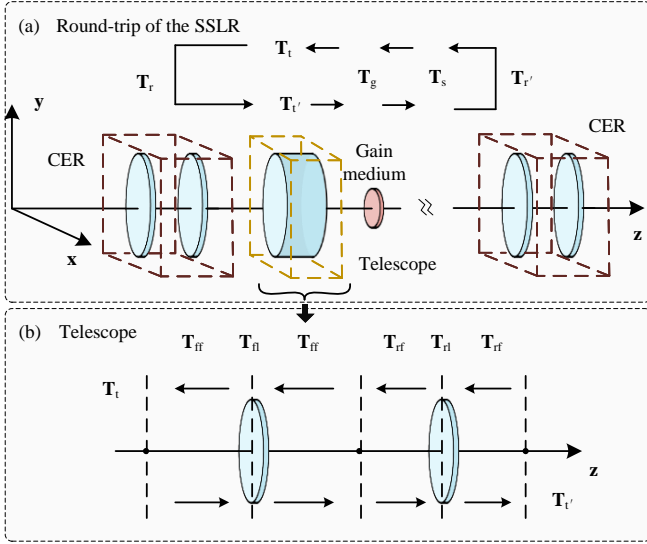


Fig. 3. Diagram of (a) SSLR round-trip and (b) telescope transmission matrix.

where

$$\omega_{00}^2(0) = \frac{\lambda L^*}{\pi} \sqrt{\frac{g_2^*}{g_1^*(1 - g_1^*g_2^*)}}, \quad (13)$$

$\omega_{00}(0)$ is the resonant beam radius at mirror M1. According to the ABCD law, we can obtain the q-parameter of the resonant beam at the gain medium $q(l_1 + f_1)$ from $q(0)$

$$q(l_1 + f_1) = \frac{-\frac{\Delta_1}{f_1}q(0) + l_1}{-\frac{1}{f_1}q(0) + 1}. \quad (14)$$

Furthermore, we can calculate the TEM₀₀ mode radius of the resonant beam at the gain medium as

$$\omega_{00}(l_1 + f_1) = \sqrt{-\frac{\lambda}{\pi \text{Im}[1/q(l_1 + f_1)]}}, \quad (15)$$

where $\text{Im}[\cdot]$ represents the imaginary part of a complex number.

D. Energy transfer performance analysis

To analyze the resonant beam optical power of the RBS system, we need to determine the losses within the SSLR when the receiver moves. These losses mainly consist of two parts: 1) the diffraction efficiency η_t of the resonant beam for a round trip within the cavity; 2) The resonant beam's scattering and absorption losses η_s inside the gain medium, lenses, and mirrors. Once the internal cavity losses are determined, the resonant beam intensity within the cavity can be calculated using the circulating power model [36].

1) *Diffraction loss calculation*: Firstly, we solve the transmission losses within the resonant cavity by establishing a mathematical model for the proposed system. As illustrated in Fig. 3(a), we define the gain medium as the $Z = 0$ plane and $u(x, y, z_0)$ as the transverse mode distribution of the resonant light at the $Z = z_0$ plane. We adopt the angular spectrum theory of beam transmission [37] and the Fox-Li iterative method [38] to solve for the stable transverse mode distribution

of the resonant beam. The round-trip transmission process of the resonant beam within the cavity can be represented by a self-consistent equation

$$\begin{aligned} \gamma \mathbf{u} &= \mathbf{T} \mathbf{u} \\ \mathbf{u} &= \mathbf{u}(x, y, 0)^T, \mathbf{T} = \mathbf{T}_g \mathbf{T}_s \mathbf{T}_r' \mathbf{T}_s \mathbf{T}_g \mathbf{T}_t' \mathbf{T}_r \mathbf{T}_t \end{aligned}, \quad (16)$$

where γ is the eigenvalue indicating the field change with one round-trip transmission. By solving the self-consistent equation, we can obtain the value of γ and subsequently calculate the intra-cavity diffraction efficiency $\eta_t = |\gamma|^2$. \mathbf{T}_g , \mathbf{T}_r , \mathbf{T}_r' , \mathbf{T}_s , and \mathbf{T}_s' are the transmission matrices of the optical field transfer through gain medium, CER at transmitter, CER at receiver, and free space from the receiver pupil to transmitter pupil, respectively, which are given in [39]. \mathbf{T}_t denotes the transmission matrix of the internal telescope within the cavity, and \mathbf{T}_t' denotes the transmission matrix of the reverse telescope as in Fig. 3(b), which can be expressed as

$$\mathbf{T}_t = \mathbf{T}_{ff} \mathbf{T}_{fl} \mathbf{T}_{ff} \mathbf{T}_{rf} \mathbf{T}_{r1} \mathbf{T}_{rf}, \quad (17)$$

$$\mathbf{T}_t' = \mathbf{T}_{rf} \mathbf{T}_{r1} \mathbf{T}_{rf} \mathbf{T}_{ff} \mathbf{T}_{fl} \mathbf{T}_{ff}, \quad (18)$$

where \mathbf{T}_{fl} and \mathbf{T}_{r1} are the transition matrices for field transfer through lens L3 and lens L4, respectively. \mathbf{T}_{ff} and \mathbf{T}_{rf} are the transition matrices for field transfer through the free space with distances f_3 and f_4 , respectively. The corresponding optical field transmission operations can be expressed as

$$\begin{aligned} \mathbf{T}_{r1} \mathbf{u} &= [u(x, y) L_1(x, y)]^T \\ \mathbf{T}_{fl} \mathbf{u} &= [u(x, y) L_2(x, y)]^T \\ \mathbf{T}_{rf} \mathbf{u} &= [\mathcal{F}^{-1} \{ \mathcal{F} \{ u(x, y) \} H(v_x, v_y; f_3) \}]^T, \\ \mathbf{T}_{ff} \mathbf{u} &= [\mathcal{F}^{-1} \{ \mathcal{F} \{ u(x, y) \} H(v_x, v_y; f_4) \}]^T \end{aligned}, \quad (19)$$

where $H(v_x, v_y; f_3)$ and $H(v_x, v_y; f_4)$ are the free space propagation kernel of the field mode. $L_1(x, y)$ and $L_2(x, y)$ represent the phase changes after the field passes through lens L3 and lens L4, respectively. Through the Fox-Li iterative method, we can obtain the transverse mode distribution of the resonant beam in the gain medium in the stable state and the eigenvalue γ of Equation (16). The diffraction loss η_t can be obtained according to γ .

2) *Scattering and absorption losses analysis*: Since the reflective or transmissive coatings on the surfaces of the optical components exhibit different reflectivity and transmittance with varying incident angles, each optical component's reflectivity and transmittance vary with different incident angles, especially at the gain medium. In our model, we consider the loss factor η_s as the product of η_c and η_g , where η_c represents a constant that does not change with the incident angle, and η_g represents a loss factor that changes with the incident angle. The loss factor η_g is given by

$$\eta_g(\theta) = \eta_m \left(\theta_{set} + \frac{\theta}{M_t} \right), \quad (20)$$

where $\theta_{set} = 45^\circ$ is the angle between the gain medium and optical axis of the transmitter within the SSLR and $\eta_m(\cdot)$ is the transmission efficiency of the resonant beam at the gain medium. Since the front and rear surfaces of the gain medium are coated with anti-reflective and high-reflective films at 45° , the gain medium has the highest transmission efficiency at an incident angle of 45° .

3) *Transmission power calculation*: Based on the circulating power model, the intra-cavity resonant beam power P_{rb} can be depicted as [34]

$$P_{\text{rb}}(\theta) = \frac{\eta_o \eta_c \eta_g(\theta) \sqrt{\eta_t} (P_{\text{in}} - P_{\text{th}})}{\left[1 - R_{\text{out}} \sqrt{\eta_t} + \sqrt{R_{\text{out}} \eta_t} \left(\frac{1}{\eta_c \eta_g(\theta) \sqrt{\eta_t}} - \eta_s \right) \right]}, \quad (21)$$

where

$$P_{\text{th}} = \frac{a_g I_s \left| \ln \sqrt{R_{\text{out}} \eta_c^2 \eta_g^2(\theta) \eta_t} \right|}{\eta_e}, \quad (22)$$

I_s is the saturation intensity, R_{out} is the reflectivity of the output mirror M2, η_o is the overlapping efficiency, P_{th} is the power threshold of the input pump power, a_g is the radius of the stimulated gain medium, and η_e is the pump efficiency.

The intra-cavity resonant beam is then released by mirror M2 partially and collected by the PV, and converted into electrical energy to charge the device battery. The PV panel can be equivalent to a current source parallel to a diode. When a load with resistance R_L is connected to the PV panel, the output electrical power P_{pt} can be obtained as:

$$\begin{cases} I_p = \eta_{\text{pv}}(1 - R_{\text{out}})P_{\text{rb}} \\ P_{\text{pt}} = I_{\text{out}}^2 R_L \\ I_{\text{out}} = I_p - I_0 \left[e^{\frac{I_{\text{out}} q (R_L + R_s)}{k T n n_s}} - 1 \right] - \frac{I_{\text{out}} (R_L + R_s)}{R_{\text{sh}}} \end{cases}, \quad (23)$$

where η_{pv} is the responsivity of PV, q is the electron charge, T is the temperature of the environment, k is the Boltzmann constant, I_0 is the reverse saturation current, n is the diode ideality factor, and n_s is the number of cells inside the PV panel. R_s and R_{sh} are the series resistance and the shunt resistance in the equivalent PV panel model, respectively. Utilizing a maximum power point tracking device, the load resistance R_L of the PV can be adjusted to track the maximum power point of the PV, thus maximizing the electrical power P_{pv} outputting at the receiver.

E. Communication performance analysis

When the intra-cavity resonant beam passes through the SHG crystal, part of the resonant beam is converted into the frequency-doubled beam and is modulated after passing through the modulator. We use quadrature amplitude modulation (QAM) and optical orthogonal frequency division Multiplexing (O-OFDM) techniques to achieve signal modulation. We implement signal modulation and demodulation using intensity modulation and direct detection (IM/DD) methods. By applying Hermitian symmetry to the QAM symbol blocks, the OFDM signal generated by the IFFT operation is converted into a real-valued signal for use in the IM/DD system. At this point, the spectral efficiency C of the system can be expressed as [10]

$$C = \frac{\frac{1}{2} N_{\text{fft}} \sum_{k=1}^{\frac{1}{2} N_{\text{fft}}} \log_2(M_k)}{N_{\text{fft}} + N_{\text{cp}}}, \quad (24)$$

where N_{fft} is the FFT size, M_k is the constellation size modulated on the subcarrier with index k , N_{cp} is the OFDM

cyclic prefix length. The communication rate W of the system can be calculated as

$$R = W_b C, \quad (25)$$

where W_b is the bandwidth of the EOM. To ensure that the communication capacity can meet the requirements for transmitting the modulated signal, the condition to be satisfied can be expressed as [40]

$$\begin{cases} C < \frac{1}{2} \log_2 \left[1 + \frac{(\eta_{\text{pv}} P_{\text{it}})^2}{2\pi e R_b \left(2q I_{\text{bg}} + \frac{4kT}{R_L} + 2q \eta_{\text{pv}} P_{\text{it}} \right)} \right] \\ P_{\text{it}} = \frac{8\pi d_{\text{eff}}^2 l_s^2}{\varepsilon_0 c \lambda^2 n_0^3 \omega_s^2} P_{\text{rb}} \end{cases} \quad (26)$$

where P_{it} is the power of the frequency-doubled beam, e is the nature constant, k is the Boltzmann constant, q is the elementary charge, I_{bg} is the background irradiance, T is the temperature, and R_L is the load resistance of the receiver circuit, d_{eff} is the SHG crystal's efficient nonlinear coefficient, l_s is the thickness of the SHG crystal, n_0 is the refractive index of the SHG crystal, ε_0 is the vacuum permeability, c is the speed of light, ω_s is the resonant beam radius on the SHG crystal.

III. SYSTEM OPTIMIZATION

In this section, we define and discuss the RB-SLIPT system's achievable performance region of the communication capacity, transmission power, and FoV performance. In addition, an optimization method for the resonant beam transmission system is proposed, which can be used to calculate the Pareto front of the system's achievable performance range.

A. Achievable Performance Region

The performance of the RB-SLIPT system encompasses energy transfer power P_{pt} , communication rate W , and FoV θ_{max} . To characterize the power transfer and communication performance of the system under mobile conditions, we define the system's FoV θ_{max} , average power transfer efficiency η_{avg} , and average communication rate R_{avg} , which can be expressed as

$$\theta_{\text{max}} = \max \{ \theta_{\text{tx}} | P_{\text{pt}}(\theta_{\text{tx}}) > 0 \} \quad (27)$$

$$\eta_{\text{avg}} = \int_{-\frac{\theta_{\text{max}}}{2}}^{\frac{\theta_{\text{max}}}{2}} \frac{P_{\text{pt}}(\theta_{\text{tx}})}{\theta_{\text{max}} P_{\text{in}}} d\theta_{\text{tx}} \quad (28)$$

$$R_{\text{avg}} = \int_{-\frac{\theta_{\text{max}}}{2}}^{\frac{\theta_{\text{max}}}{2}} \frac{W(\theta_{\text{tx}})}{\theta_{\text{max}}} d\theta_{\text{tx}} \quad (29)$$

By calculating the maximum off-axis angle θ_{tx} at which the SSLR can maintain stable oscillation, θ_{max} can be determined. Within the FoV, the resonant beam is proportionally divided into communication and power transfer beams by SHG crystals. The power of the 532-nm beam used for communication and the 1064-nm beam used for energy transfer affect the system's communication and energy transfer performance. These two performance metrics are interdependent, such that an increase in one often results in a decrease in the other. By calculating η_{avg} and R_{avg} within the system's FoV, the overall performance of the system can be effectively characterized.

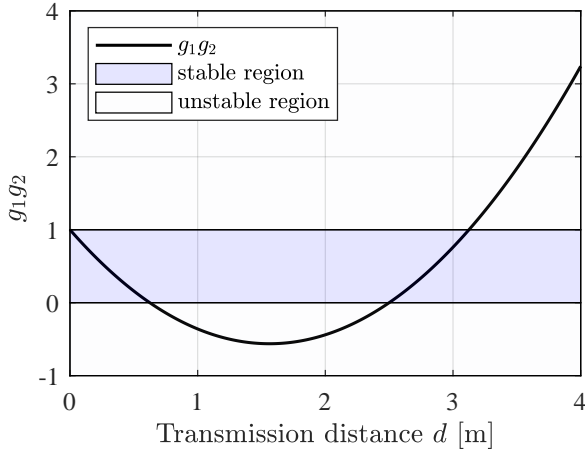


Fig. 4. The stable range of the SSLR.

According to Equation (21), the intra-cavity resonant beam varies with changes in parameters $\eta_o, \eta_c, \eta_g, \eta_t, a_g,$ and R_{out} , thereby affecting P_{it}, P_{pt} at different angles. This variation also impacts the threshold pump power, influencing θ_{max} . Among these parameters, η_o, η_c, η_g are intrinsic to the optical components. Thus, we can enhance system performance by adjusting the values of η_t, a_g and R_{out} . By altering the system structural parameter $(f_1, f_2, f_3, f_4, l_1, l_2)$ of the SSLR, we can modify the modes of the resonant beam in the cavity, which in turn changes η_t . In addition, M_t changes the loss η_g under different incident angles of the resonant beam, which also affects the system performance. From the analysis of equivalent resonant cavities, it has been observed that an SSLR can be effectively modeled as a double-concave stable cavity composed of two concave mirrors. The radii of curvature f_{R1} and f_{R2} of the equivalent concave mirrors are determined by the parameters (f_1, f_3, f_4, l_1) and (f_2, l_2) , respectively. Consequently, the system parameter \mathbf{v}_1 can be simplified as

$$\mathbf{v}_1 = (f_{R1}, f_{R2}, M_t, a_g, R, l_s). \quad (30)$$

As the system parameters change, the stability region of the SSLR varies, resulting in the discontinuous stability region shown in Fig.4. To ensure the system's proper functioning, it is necessary to eliminate this issue, ensuring that the stability region is continuous and completely covers the maximum operating distance. Therefore, the set of feasible RB-SLIPT system parameters \mathbf{v}_1 selecting strategies S considering stability constraints can be formulated as

$$S = \{f_{R1}, f_{R2}, M_t, a_g, R, l_s\} : \forall d \in [0, d_{max}], 0 < g_1 g_2 < 1, \quad (31)$$

where d_{max} is the maximum operation distance of the RB-SLIPT system.

Definition 1 (Achievable performance region): The achievable performance region $\mathcal{R} \subseteq \mathbb{R}_+^3$ is defined as

$$\mathcal{R} = \{\eta_{avg}, \theta_{max}, R_{avg}\} : \forall \{f_{R1}, f_{R2}, M_t, a_g, R\} \in S \quad (32)$$

For the RB-SLIPT system, points within set \mathcal{R} that offer superior performance lie on the Pareto front of the set \mathcal{R} , as

follows. Therefore, we should determine the Pareto front of the set \mathcal{R} to optimize the system.

Definition 2 (Pareto front): A point \mathbf{x} is called Pareto optimal solution of a set P , if $\mathbf{x} \in P$ while $\mathbf{x}' \in \mathbb{R}_+^L$ satisfying $\mathbf{x}' > \mathbf{x}$ with an element-wise inequality not in set P . The set of all Pareto optimal solutions is called the Pareto front of the set P .

B. RB-SLIPT system Optimization

Based on the analysis above, the system optimization problem can be transformed into maximizing the average transmission efficiency η_{avg} , average communication rate R_{avg} , and θ_{max} , which can be expressed as

$$\begin{aligned} \text{P1} : \quad & \max_{\mathbf{v}_1 \in \mathbb{R}_+^6} \{\theta_{max}, \eta_{avg}, R_{avg}\} \\ \text{s.t.} \quad & 0 < g_1 g_2 < 1, \forall d \in [0, d_{max}], \\ & P_{in} = P_{set}. \end{aligned} \quad (33)$$

where P_{set} is the predetermined pump light intensity. We set $d_{max} = 6$ because a maximum operating distance of 6 m can satisfy the needs of the majority of SLIPT applications. The frequency-doubled beam's optical power determines the system's communication capacity. However, once the optical power of the frequency-doubled beam reaches a certain level, the communication rate of the system becomes constrained by the modulator's bandwidth and modulation format. Therefore, we transform Problem (P1) into an optimization problem for θ_{max} and η_{avg} , subject to the constraint of meeting the communication rate requirements:

$$\begin{aligned} \text{P1}^* : \quad & \max_{\mathbf{v}_1 \in \mathbb{R}_+^6} \{\theta_{max}, \eta_{avg}\} \\ \text{s.t.} \quad & 0 < g_1 g_2 < 1, \forall d \in [0, d_{max}], \\ & R_{avg} \geq R_{lb}, \\ & P_{in} = P_{set}. \end{aligned} \quad (34)$$

where R_{lb} is the lower bound of the system's communication rate. Due to many parameter variables in \mathbf{v}_1 , we decompose the problem into three independent sub-problems: 1) optimizing the loss factor η_t under a fixed M_t ; 2) optimizing η_{avg} and θ_{max} ; 3) calculating the minimum SHG crystal size that ensures the average communication rate R_{avg} exceeds R_{lb} .

1) *Optimization of loss factor η_t :* In the SSLR, the loss factor η_t primarily includes losses from resonant beam propagation through air and diffraction losses through optical components. The transmission losses of resonant beams in air are relatively minor and are generally considered solely related to transmission distance. The majority of intra-cavity losses arise from diffraction losses through optical components. Using larger-radius optical lenses and mirrors can reduce diffraction losses significantly, especially when the radius is two to three times larger than the radius of the resonant beam's beam spot. Typically, the beam spot radius of the resonant beam is on the millimeter scale, while the radii of standard lenses and mirrors are on the centimeter scale. Hence, diffraction losses at the lenses and mirrors are minimal. However, at the gain medium, increasing the radius of the gain medium requires a larger pump light spot area to achieve

pumping of the gain medium, which reduces the power density of the pump light, thereby decreasing the pumping efficiency. Therefore, optimizing the structure of the resonator to reduce the beam spot radius at the gain medium can decrease intra-cavity transmission losses and enhance system transmission efficiency η_t .

In a specific application scenario, the relative distance between the transmitter and the receiver is generally stable. Therefore, we optimize the system structure for a predetermined transmission distance d_{set} . By setting M_t as a fixed value M_{set} , we minimize the size of the resonant beam spot at the gain medium by optimizing the parameter (f_{R1}, f_{R2}) . The optimization problem for the resonant beam spot aperture can be expressed as

$$\begin{aligned} \text{P1.1: } & (f_{R1}^*, f_{R2}^*) = \arg \min_{(f_{R1}, f_{R2})} \omega_g \\ \text{s.t. } & 0 < g_1 g_2 < 1, \forall d \in [0, 6], \\ & d = d_{\text{set}}, \\ & M_t = M_{\text{set}}. \end{aligned} \quad (35)$$

2) *Optimization of transmission efficiency and FoV*: With the confirmed structure of the transceiver's retro-reflector, it is essential to optimize the radius of the gain medium further a_g , the output efficiency of the output mirror R_{out} , and the telescope lens ratio M_t within the SSLR to enhance system performance. M_t affects the intra-cavity diffraction losses η_t of the SSLR at different radial angles; a_g influences the diffraction losses of the resonant beam on the gain medium Γ_g and the small-signal gain coefficient g_0 of the gain medium; R_{out} directly impacts the system's end-to-end transmission efficiency η_{avg} and the threshold of the pump light intensity P_{th} . We need to further adjust these three parameters to optimize η_{avg} and θ_{max} which can be formulated as

$$\begin{aligned} \text{P1.2: } & a_g^*, R_{\text{out}}^*, M_t^* = \arg \max_{a_g, R_{\text{out}}, M_t} \{\eta_{\text{avg}}, \theta_{\text{max}}\} \\ \text{s.t. } & f_{R1}, f_{R2} = f_{R1}^*, f_{R2}^*, \\ & l_s = l_{\text{set}}, \end{aligned} \quad (36)$$

where l_{set} is the preset thickness of the SHG crystal. Since the loss of the intra-cavity resonant beam caused by the SHG crystal is relatively small and do not have a significant impact on η_{avg} and θ_{max} , the system communication performance can be optimized separately from the system's energy transfer and FoV performance.

3) *SHG crystal size calculation*: By solving Problem (P1.1) and Problem (P1.2) separately, we reduced the intra-cavity transmission loss by minimizing the resonant beam spot radius. Further, we selected suitable a_g, R_{out}, M_t to maximize η_{avg} and θ_{max} . Based on the optimized resonator parameters, we then determined the minimum SHG crystal size required to ensure that the system's communication rate met the minimum communication requirements, which can be expressed as

$$\begin{aligned} \text{P1.3: } & l_s^* = \arg \min_{l_s} \{|R_{\text{avg}} - R_{\text{lb}}|\} \\ \text{s.t. } & f_{R1}, f_{R2} = f_{R1}^*, f_{R2}^*, \\ & a_g, R_{\text{out}}, M_t = a_g^*, R_{\text{out}}^*, M_t^*. \end{aligned} \quad (37)$$

By decomposing the optimization problem (P1*) into three sub-problems, the dimensionality of the independent variable space is effectively reduced. Consequently, the sub-problems can be addressed individually through grid search, ultimately yielding the solution to the problem (P1*). The specific algorithm for solving this problem can be given by Algorithm 1. M_P obtained through algorithmic solution represents the Pareto front of the achievable performance region S , while M_{V_1} consists of the collection of system parameters \mathbf{v} that correspond to system performance in M_P .

Algorithm 1: Grid Search to Optimize RBS

```

Input:  $d_{\text{set}}, \Delta_{\text{max}}, M_{\text{max}}, a_{\text{max}}$ 
1 Initialize  $M_1, M_{\text{res}}, M_v, M_p, \theta_{\text{max}}, \omega_{\text{min}}$ ;
  // Solve Problem (P1.1)
2 for  $\Delta_1 = 0$  to  $\Delta_{\text{max}}$  do
3   for  $\Delta_2 = 0$  to  $\Delta_{\text{max}}$  do
4     Calculate  $f_{R1}, f_{R2}$  according to (6)&(7);
5     if  $\omega_g(f_{R1}, f_{R2}) < \omega_{\text{min}}$  then
6        $\omega_{\text{min}} = \omega_g(f_{R1}, f_{R2})$ ;
7        $f_{\text{res}1}, f_{\text{res}2} = f_{R1}, f_{R2}$ ;
8     end
9   end
10 end
  // Solve Problem (P1.2)
11 for  $M_t = 0$  to  $M_{\text{max}}$  do
12   Calculate  $\eta_t$  at different radial angles;
13    $M_1.append((f_{R1}, f_{R2}, \eta_t, M_t))$ ;
14 end
15 for  $itr = 1$  to  $\text{length}(M_1)$  do
16    $(f_{R1}, f_{R2}, \eta_t, M_t) = M_1[itr]$ ;
17   for  $a_g = 0$  to  $a_{\text{max}}$  do
18     for  $R_{\text{out}} = 0$  to 1 do
19       Calculate  $\eta_{\text{avg}}, \theta$  according to (26)&(27);
20        $M_{\text{res}}.append((f_{R1}, f_{R2}, \eta_t, M_t, a_g, \eta_{\text{avg}}, \theta))$ ;
21     end
22   end
23 end
  // Find Pareto front of the set  $M_{\text{res}}$ 
  // Solve Problem (P1.3)
24 Sort  $M_{\text{res}}$  in descending order by the first element  $\eta_{\text{avg}}$ ;
25 for  $itr = 1$  to  $\text{length}(M_{\text{res}})$  do
26    $f_{R1}, f_{R2}, \eta_t, M_t, \eta_{\text{avg}}, \theta = M_{\text{res}}[itr]$ ;
27   if  $\theta > \theta_{\text{max}}$  then
28     Calculate  $l_s$  according to (26);
29      $M_P.append((\eta_{\text{avg}}, \theta, R_{\text{avg}}))$ ;
30      $M_v.append((f_{R1}, f_{R2}, a_g, R, M_t, l_s))$ ;
31      $\theta_{\text{max}} = \theta$ ;
32   end
33 end
Result:  $M_P, M_v$ 

```

Based on Algorithm 1, the optimization problem P1.1 is initially solved, which involves optimizing the minimum spot radius of the resonant beam at the gain medium under stable conditions by adjusting the equivalent focal length (f_{R1}, f_{R2}) . The pattern of the equivalent focal length f_{R1} and

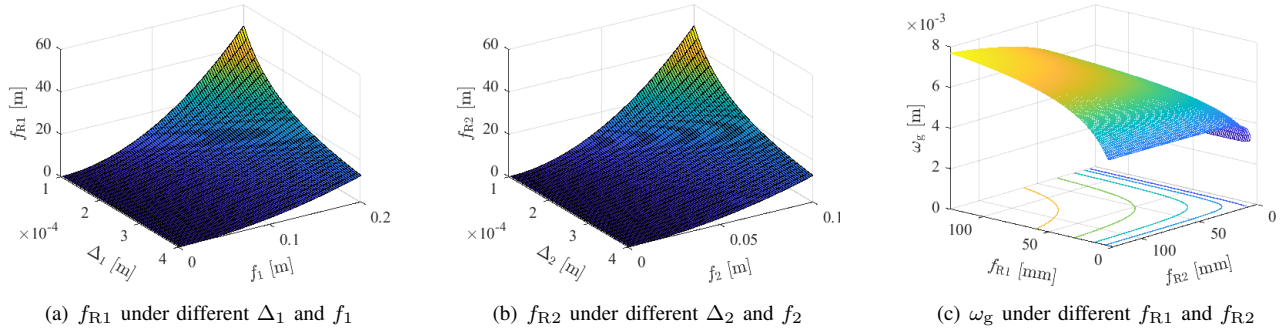


Fig. 5. Effect of (Δ_1, Δ_2) and focal length (f_1, f_2) on resonant beam spot aperture at gain medium ω_g .

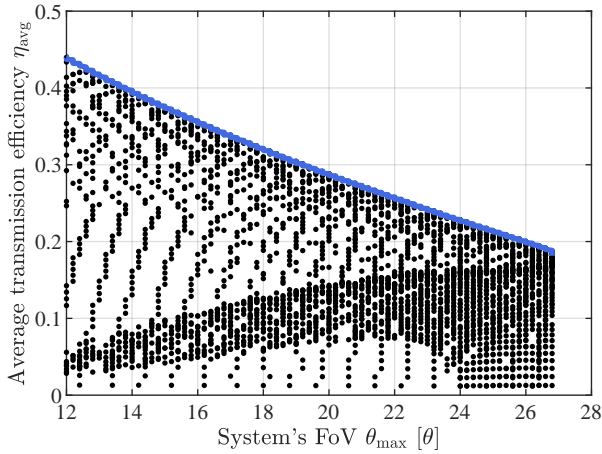


Fig. 6. Pareto front of the system's achievable performance region.

the parameters Δ_1 and f_1 is illustrated in Fig. 5(a), while the relationship between the equivalent focal length f_{R1} and the parameters Δ_2 and f_2 is depicted in Fig. 5(b). Since both parameters Δ_1 and f_1 influence f_{R1} , we maintain $f_1 = 25$ mm and vary Δ_1 to change the value of f_{R1} . Similarly, we set $f_1 = 25$ mm and control the variation in f_{R2} by changing Δ_2 . Figure 5(c) depicts the relationship between the resonant beam spot radius at the gain medium and the equivalent focal length (f_{R1}, f_{R2}) . We can obtain the minimum spot radius and the corresponding equivalent focal length through grid search, which is

$$\begin{cases} \omega_g = 1.9 \text{ mm}, \\ f_{R1}^* = 3.9063 \text{ m}, \\ f_{R2}^* = 3.0488 \text{ m}, \end{cases} \quad (38)$$

By substituting (f_{R1}^*, f_{R2}^*) into the problem (1.2) and further solving the feasible solution via grid search for the Pareto frontier, the final optimization results are shown in Fig.6. The area covered by the black dots represents the range of all feasible solutions calculated, and the blue lines represent the Pareto frontier of the feasible solutions. In the Pareto frontier set, θ_{\max} can reach up to $\pm 26.8^\circ$, and η_{avg} can reach 13.2%. Depending on different application scenarios, appropriate system parameters can be selected to design an RB-SLIPT system so that the performance can meet corresponding requirements.

IV. NUMERICAL RESULTS AND DISCUSSIONS

A. Parameters Setting

The parameters of the RB-SLIPT system are listed in Table I. We use Nd:YVO₄ crystal as the gain medium and KTP crystal to realize SHG. A 100 W semiconductor laser with a wavelength of 808-nm is used as a pump source to generate a 1064-nm energy transfer beam and a 532-nm communication carrier. At the receiver, we use InGaAsP and GaAs as the materials for PV and PD, respectively, due to their excellent responsivity at 1064-nm and 532-nm. The diameter of the intra-cavity lens and mirrors is 25.4 mm. To match the FoV of the transceiver retro-reflectors, we set the focal length of lenses L2 and L4 to 25.4 mm.

We employ 256-QAM to modulate the frequency-doubled beam and utilize O-OFDM technology to multiplex different subcarriers, with a total of $N_{\text{fft}} = 1024$ subcarriers. Under these conditions, the system's spectral efficiency $C = 3.98$ bit/s/Hz. Electro-absorption modulators can be used as the modulator of the frequency-doubled beam, whose modulation bandwidth can reach 800 MHz [41]. The system's communication rate can be achieved up to 3.18 Gbps. We can ensure that the system's signal-to-noise ratio meets the required communication standards by designing an appropriately sized frequency-doubling crystal as detailed in Section III-B1.

TABLE I
PARAMETERS IN THEORETICAL CALCULATION

Parameter	Symbol	Value
Saturation intensity	I_s	$1.26 \times 10^7 \text{ W/m}^2$
Efficient nonlinear coefficient	d_{eff}	4.7 pm/V
KTP crystal refractive index	n_0	2.23
Excitation efficiency	η_e	72%
PV's responsivity	η_{pv}	0.4 A/W
PD's responsivity spot	η_{pd}	0.4 A/W
Load resistor	R_{IL}	10 k Ω
Shunt resistance	R_{sh}	53.81 Ω
Series resistance	R_s	37 m Ω

B. Performance of the optimized resonant beam SLIPT system

Using the optimization algorithm proposed in Section III-B, we identified the Pareto frontier of the achievable performance of the system at a distance of 2 m while $P_{\text{in}} = 100$ W, as shown in Fig.7. With the increasing telescope

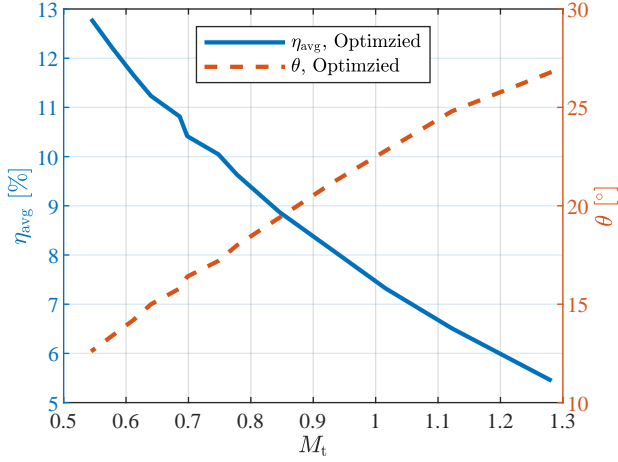


Fig. 7. Average transmission efficiency η_{avg} and FoV θ_{max} as a function of telescope ratio M_t in the Pareto front of the system's achievable performance region.

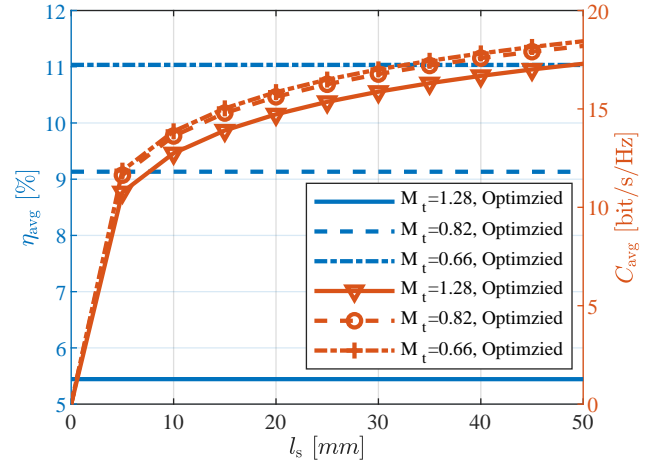


Fig. 10. Average power transfer efficiency η_{avg} and average communication capacity C_{avg} as a function of SHG crystal thickness l_s under optimized system structures.

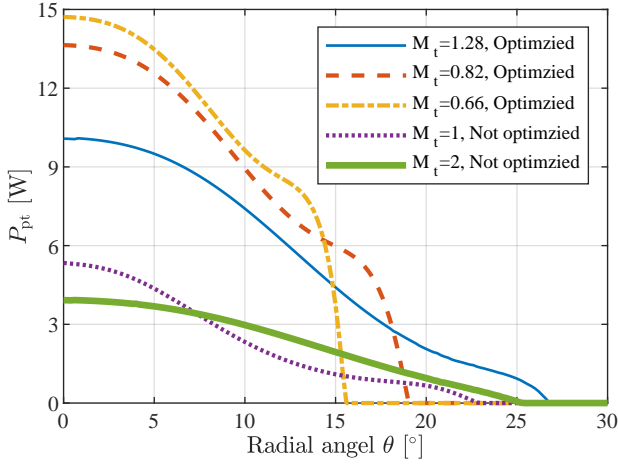


Fig. 8. Average transmission efficiency η_{avg} as a function of radial angle θ under different system structure.

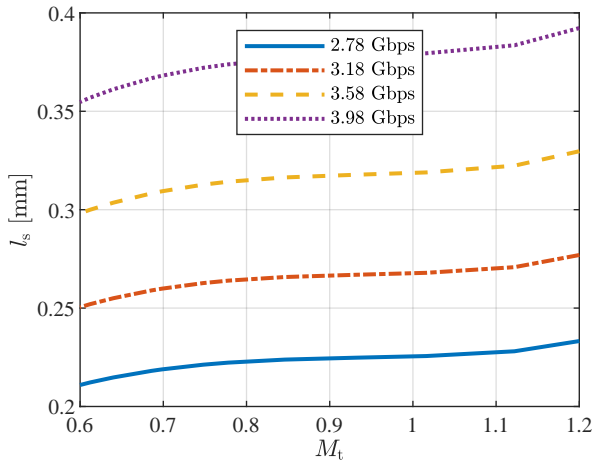


Fig. 9. SHG crystal thickness l_s as a function of telescope ratio M_t under different communication rate requirements.

lens ratio M_t , the system's average transmission efficiency η_{avg} continuously decreases, while the maximum FoV θ_{max} consistently increases. Thus, by adjusting M_t , one can select the appropriate system performance to meet various needs for transmission efficiency and FoV. Additionally, when M_t exceeds 1.28, the system's performance is no longer on the Pareto frontier. In this scenario, it is further increasing M_t neither enhances the system's FoV θ_{max} nor improves its average transmission efficiency η_{avg} . At this point, both η_{avg} and θ_{max} are inferior to those with a lower M_t . We compared the system's output electrical power P_{pt} with $M_t=1.28$, $M_t=0.82$, and $M_t=0.66$ on the Pareto frontier with the non-optimized systems with $M_t=1$ and $M_t=2$, as shown in Fig.8. The system with $M_t=0.66$, $M_t=0.82$, and $M_t=1.28$ correspond to system configurations on the Pareto frontier, representing high average transmission efficiency with lower FoV, a balanced trade-off between average transmission efficiency and FoV, and high FoV with lower average transmission efficiency, respectively. $M_t=1$ and $M_t=2$ represent system configurations without the telescope and with a telescope having a lens focal ratio of 2, respectively. Before optimization, regardless of $M_t=1$ or $M_t=2$, P_{pt} was relatively low. After optimization, the systems with lens ratios of 0.82 and 0.66 significantly improved average energy transmission power. Compared to the resonant beam SLIPT system without the telescopes (i.e., $M_t=1$), the optimized system with $M_t=0.66$ exhibits a 400% increase in average transmission efficiency. Moreover, when $M_t = 1.28$, θ_{max} reached $\pm 26.8^\circ$, and the average energy transmission efficiency η_{avg} reached 5.4%. The system's FoV and average transmission efficiency have increased by 17% and 145%, respectively, compared to the system without telescopes. During optimization, we adjusted the output efficiency of the output mirror to maximize transmission efficiency, which led to a reduction in intra-cavity light compared to before optimization, thereby decreasing the efficiency of frequency doubling and reducing the system's communication capacity.

C. Trade-off Between Power Transfer Performance and Communication Rate

Furthermore, we determined the minimum SHG crystal thickness l_s required to meet the communication rate for different telescope lens ratios M_t . Figure 9 illustrates the relationship between the required thickness of the SHG crystal l_s and the telescope lens ratio M_t under varying communication rate requirements. We employed 64 QAM, 128 QAM, 256 QAM, and 512 QAM modulation formats, achieving communication rates of 2.78 Gbps, 3.18 Gbps, 3.58 Gbps, and 3.98 Gbps, respectively. As M_t increases, the system's average transmission efficiency decreases, resulting in a reduced η_{avg} for the same l_s . Consequently, to maintain communication efficiency, a thicker SHG crystal is required. Additionally, as the communication rate increases, the required thickness of the SHG crystal correspondingly increases. In the resonant beam SLIPT system, the communication signal-to-noise ratio of the system can be improved by increasing the optical power of the optical carrier. Therefore, we can control the SHG efficiency η_{shg} by adjusting the thickness of the SHG crystal l_s , thereby increasing the communication rate of the system.

Figure 10 demonstrates the changes in energy transmission power and communication capacity under different telescope lens ratios M_t as the thickness of the SHG crystal l_s increases. As l_s increases, the system's communication capacity significantly increases, while the system's energy transmission power is not notably affected, indicating that the power of the frequency-doubled beam used for communication only occupies a small part of the resonant beam energy. When $l_s = 10$ mm, systems with lens ratios M_t of 1.28, 0.82, and 0.66, respectively, can achieve communication capacities of 13 bit/s/Hz, 14 bit/s/Hz, and 14.2 bit/s/Hz, meeting most communication needs.

V. CONCLUSIONS

This paper proposes a resonant beam simultaneous light and power transfer (SLIPT) system enhanced with a telescope. By incorporating a telescope at the transmitter, the modulator and gain medium can be spatially separated, thus simplifying the system's architecture. Our findings indicate that the system's field of view (FoV) and transmission efficiency can be modulated by adjusting the lens ratio of the telescope. Additionally, we optimized the system parameters \mathbf{v}_1 to delineate the Pareto frontier of the system's achievable performance region. As a result, the system's FoV can be extended to a maximum of $\pm 26.8^\circ$, and the average optical transmission efficiency η_{avg} can reach a maximum of 5.4%.

REFERENCES

- [1] P. D. Diamantoulakis and G. K. Karagiannidis, "Simultaneous lightwave information and power transfer (slipt) for indoor iot applications," in *IEEE Global Communications Conference*, Dec. 2017, pp. 1–6.
- [2] P. D. Diamantoulakis, G. K. Karagiannidis, and Z. Ding, "Simultaneous lightwave information and power transfer (SLIPT)," *IEEE Trans. Green Commun. Netw.*, vol. 2, no. 3, pp. 764–773, Mar. 2018.
- [3] S. S. Morapitiya, M. F. Ali, S. Rajkumar, S. K. Wijayasekara, D. N. K. Jayakody, and R. Weerasuriya, "A SLIPT-assisted visible light communication scheme," in *2020 16th International Conference on Distributed Computing in Sensor Systems (DCOSS)*. IEEE, May 2020, pp. 368–375.
- [4] G. A. Ropokis and P. S. Bithas, "Wireless powered relay networks: Rate optimal and power consumption-aware wpt/swipt," *IEEE Trans. Veh. Technol.*, vol. 71, no. 8, pp. 8574–8590, Aug. 2022.
- [5] A. Jahid, M. H. Alsharif, and T. J. Hall, "A contemporary survey on free space optical communication: Potentials, technical challenges, recent advances and research direction," *J. Netw. Comput. Appl.*, vol. 200, p. 103311, Apr. 2022.
- [6] K. W. Palitharathna, N. D. Wickramasinghe, A. M. Vegni, and H. A. Suraweera, "Neural network-based optimization for SLIPT-enabled indoor VLC systems with energy constraints," *IEEE Trans. Green Commun. Netw.*, vol. 8, no. 2, pp. 839–851, Dec. 2024.
- [7] H. Haas, "LiFi is a paradigm-shifting 5G technology," *Rev. Phys.*, vol. 3, pp. 26–31, Nov. 2018.
- [8] J. Liu, A. Wang, Q. Sheng, Y. Qi, S. Wang, M. Wang, D. Xu, S. Fu, W. Shi, and J. Yao, "Large-range alignment-free distributed-cavity laser based on an improved multi-lens retroreflector," *Chin. Opt. Lett.*, vol. 20, no. 3, p. 031407, Feb. 2022.
- [9] Q. Sheng, J. Geng, Z. Chang, A. Wang, M. Wang, S. Fu, W. Shi, and J. Yao, "Adaptive wireless power transfer via resonant laser beam over large dynamic range," *IEEE Internet Things J.*, vol. 10, no. 10, pp. 8865–8877, Dec. 2022.
- [10] D. Tsonev, S. Videv, and H. Haas, "Towards a 100 Gb/s visible light wireless access network," *Opt. Express*, vol. 23, no. 2, pp. 1627–1637, Jan. 2015.
- [11] M. Obeed, A. M. Salhab, M.-S. Alouini, and S. A. Zummo, "On optimizing VLC networks for downlink multi-user transmission: A survey," *IEEE Commun. Surv. Tutor.*, vol. 21, no. 3, pp. 2947–2976, Mar. 2019.
- [12] C. Carvalho and N. Paulino, "On the feasibility of indoor light energy harvesting for wireless sensor networks," *Procedia Technol.*, vol. 17, pp. 343–350, Oct. 2014.
- [13] C. Li, W. Jia, Q. Tao, and M. Sun, "Solar cell phone charger performance in indoor environment," in *IEEE 37th Annual Northeast Bioengineering Conference (NEBEC)*, 2011, pp. 1–2.
- [14] T. Rakia, H.-C. Yang, F. Gebali, and M.-S. Alouini, "Optimal design of dual-hop VLC/RF communication system with energy harvesting," *IEEE Commun. Lett.*, vol. 20, no. 10, pp. 1979–1982, July 2016.
- [15] M. T. Hossan, M. Z. Chowdhury, M. Shahjalal, and Y. M. Jang, "Human bond communication with head-mounted displays: Scope, challenges, solutions, and applications," *IEEE Commun. Mag.*, vol. 57, no. 2, pp. 26–32, Feb. 2019.
- [16] T. Nguyen, A. Islam, T. Hossan, and Y. M. Jang, "Current status and performance analysis of optical camera communication technologies for 5G networks," *IEEE Access*, vol. 5, pp. 4574–4594, Mar. 2017.
- [17] M. S. Bashir, "Free-space optical communications with detector arrays: A mathematical analysis," *IEEE Trans. Aerosp. Electron. Syst.*, vol. 56, no. 2, pp. 1420–1429, Apr. 2020.
- [18] N.-L. Nguyen, K.-H. Nguyen, J. Nadeem, and J. Ha, "Dynamic beam steering for wireless optical power transfer in iot applications," *Opt. Lett.*, vol. 49, no. 8, pp. 2025–2028, Apr. 2024.
- [19] A. M. Abdelhady, O. Amin, B. Shihada, and M.-S. Alouini, "Spectral efficiency and energy harvesting in multi-cell SLIPT systems," *IEEE Trans. Wirel. Commun.*, vol. 19, no. 5, pp. 3304–3318, Feb. 2020.
- [20] S. Sepehrvand, L. N. Theagarajan, and S. Hranilovic, "Rate-power trade-off in simultaneous lightwave information and power transfer systems," *IEEE Commun. Lett.*, vol. 25, no. 4, pp. 1249–1253, Dec. 2020.
- [21] Z. Zhang, Y. Xiao, Z. Ma, M. Xiao, Z. Ding, X. Lei, G. K. Karagiannidis, and P. Fan, "6G wireless networks: Vision, requirements, architecture, and key technologies," *IEEE Veh.*

- Technol. Mag.*, vol. 14, no. 3, pp. 28–41, Sept. 2019.
- [22] D. Powell *et al.*, “Lasers boost space communications,” *Nature*, vol. 499, no. 7458, pp. 266–267, July 2013.
- [23] Q. Zhang, W. Fang, Q. Liu, J. Wu, P. Xia, and L. Yang, “Distributed laser charging: A wireless power transfer approach,” *IEEE Internet Things J.*, vol. 5, no. 5, pp. 3853–3864, June 2018.
- [24] Q. Liu, M. Xiong, M. Liu, Q. Jiang, W. Fang, and Y. Bai, “Charging a smartphone over the air: The resonant beam charging method,” *IEEE Internet Things J.*, vol. 9, no. 15, pp. 13 876–13 885, Jan. 2022.
- [25] R. Beer, “Paraxial ray analysis of a cat’s-eye retroreflector: comments,” *Applied Optics*, vol. 15, no. 4, pp. 856–857, Apr. 1976.
- [26] G. Zhou, A. J. Alfrey, and L. W. Casperson, “Modes of a laser resonator with a retroreflecting corner cube mirror,” *Applied Optics*, vol. 21, no. 9, pp. 1670–1674, May 1982.
- [27] M. Liu, M. Xiong, Q. Liu, S. Zhou, and H. Deng, “Mobility-enhanced simultaneous lightwave information and power transfer,” *IEEE Trans. Wirel. Commun.*, vol. 20, no. 10, pp. 6927–6939, May 2021.
- [28] Q. Sheng, M. Wang, H. Ma, Y. Qi, J. Liu, D. Xu, W. Shi, and J. Yao, “Continuous-wave long-distributed-cavity laser using cat-eye retroreflectors,” *Opt. Express*, vol. 29, no. 21, pp. 34 269–34 277, Oct. 2021.
- [29] N. Javed, N.-L. Nguyen, S. F. A. Naqvi, and J. Ha, “EDFA-enabled resonance beam charging at 1550 nm for improved efficiency, safety, and performance,” in *Advanced Lasers, High-Power Lasers, and Applications XIV*, vol. 12760. SPIE, Nov. 2023, pp. 172–176.
- [30] M. Xiong, Q. Liu, and S. Zhou, “Optimization of a mobile optical SWIPT system with asymmetric Spatially separated laser resonator,” *IEEE Trans. Wirel. Commun.*, vol. 21, no. 11, pp. 9056–9067, Nov. 2022.
- [31] M. Xiong, M. Liu, Q. Jiang, J. Zhou, Q. Liu, and H. Deng, “Retro-reflective beam communications with spatially separated laser resonator,” *IEEE Trans. Wirel. Commun.*, vol. 20, no. 8, pp. 4917–4928, Mar. 2021.
- [32] M. Xiong, Q. Liu, S. Zhou, S. Han, and M. Liu, “Performance of a high power and capacity mobile SLIPT scheme,” *IEEE Trans. Commun.*, vol. 70, no. 7, pp. 4717–4730, July 2022.
- [33] S. Han, W. Fang, M. Liu, M. Xu, S. Xia, and Q. Liu, “Field of view expansion for resonant beam information and power transfer,” 2024. [Online]. Available: <https://arxiv.org/abs/2408.04274>
- [34] W. Koechner, *Solid-State Laser Engineering, 6th ed.* New York, NY, USA: Springer, 2006.
- [35] A. E. Siegman, *Lasers*. Mill Valley, CA: University Science Books, 1986.
- [36] N. Hodgson and H. Weber, *Laser Resonators and Beam Propagation: Fundamentals, Advanced Concepts and Applications 2nd ed.* New York, NY., U.S.: Springer, 2005.
- [37] J. W. Goodman, *Introduction to Fourier Optics, 3rd ed.* Greenwood village, U.S.: Ben Roberts, 2005.
- [38] P. Baues, “Huygens’ principle in inhomogeneous, isotropic media and a general integral equation applicable to optical resonators,” *Opto-Electron.*, vol. 1, no. 1, pp. 37–44, Jan. 1969.
- [39] Q. Liu, M. Xiong, M. Liu, Q. Jiang, W. Fang, and Y. Bai, “Charging a smartphone over the air: The resonant beam charging method,” *IEEE Internet Things J.*, vol. 9, no. 15, pp. 13 876–13 885, Jan. 2022.
- [40] A. Lapidoth, S. M. Moser, and M. A. Wigger, “On the capacity of free-space optical intensity channels,” *IEEE Trans. Inf. Theory*, vol. 55, no. 10, pp. 4449–4461, Sept. 2009.
- [41] C. Quintana, Q. Wang, D. Jakonis, X. Piao, G. Erry, D. Platt, Y. Thueux, A. Gomez, G. Faulkner, H. Chun *et al.*, “High speed electro-absorption modulator for long range retroreflective free space optics,” *IEEE Photonics Technol. Lett.*, vol. 29, no. 9, pp. 707–710, Mar. 2017.